Chlorine-doped n-type CdS nanowires with enhanced photoconductivity

To cite this article: Chunyan Wu *et al* 2010 *Nanotechnology* **21** 505203

Nanotechnology **21** (2010) 505203 (7pp) doi:10.1088/0957-4484/21/50/505203

Chlorine-doped n-type CdS nanowires with enhanced photoconductivity

Chunyan Wu[1], Jiansheng Jie[1,3], Li Wang[1], Yongqiang Yu[1,2], Qiang Peng[1], Xiwei Zhang[1], Jiajun Cai[1], Huier Guo[1], Di Wu[2] and Yang Jiang[2]

[1] School of Electronic Science and Applied Physics, Hefei University of Technology, Hefei, Anhui 230009, People's Republic of China
[2] School of Materials Science and Engineering, Hefei University of Technology, Hefei, Anhui 230009, People's Republic of China

E-mail: jason.jsjie@gmail.com

Received 17 August 2010, in final form 14 October 2010
Published 23 November 2010
Online at stacks.iop.org/Nano/21/505203

Abstract
Cl-doped n-type CdS NWs with single-crystal wurtzite structure and $[2\bar{1}\bar{1}1]$ growth direction were synthesized by using $CdCl_2$ as the dopant via a thermal co-evaporation method. By controlling the Cl vapor pressure during the growth, the conductivity of the CdS:Cl NWs can be tuned in a wide range of five orders of magnitude. A nano-photodetector based on the CdS:Cl NWs shows high sensitivity to visible light with excellent stability and reproducibility. Significantly, the photoconductivity of the CdS NWs is greatly enhanced by Cl doping and the responsivity and photoconductive gain of the CdS:Cl NWs have substantially increased compared with the undoped CdS NWs. Further study also demonstrates the polarization-dependent photoconductivity of the CdS:Cl NWs. It is expected that the CdS:Cl NWs with tunable optoelectronic properties will have important applications in high-performance nano-optoelectronic devices.

(Some figures in this article are in colour only in the electronic version)

1. Introduction

CdS, which is an important II–VI group semiconductor with a wide direct bandgap of 2.42 eV in the visible range at 300 K, has attracted considerable attention owing to its unique properties such as strong emission in the visible range [1], excellent photoconductive characteristics [2] and adjustable bandgap (1.7–3.68 eV) by alloying with other II–VI compounds, e.g. CdS_xSe_{1-x}, $Zn_xCd_{1-x}S$ and $Zn_xCd_{1-x}Se$ [3]. CdS has been widely used in diverse fields, such as optically and electrically driven laser emission [4], photovoltaics (PV) [5] and bio-imaging [6]. Recently, many efforts have been made to synthesize CdS nanostructures and explore their applications in new-generation nano-electronics and nano-optoelectronics [7]. For instance, laser emission from a single CdS nanoribbon (NR) with low threshold value has been investigated [1] and high-performance nano-field-effect transistors (nano-FETs) and nano-photoswitches have been constructed based on the CdS NR/nanowires (NWs) [2, 8, 9], revealing the great promise of CdS nanostructures as building blocks for future nano-electronic and nano-optoelectronic applications.

As we know, CdS itself is a non-stoichiometric n-type semiconductor. Its n-type characteristic mainly arises from the small amount of intrinsic donor defects such as S vacancies and Cd interstitials in it. However, since many factors such as growth conditions and the annealing process can result in a change of the donor defects, it is difficult to rationally control the transport properties of CdS by adjusting the amount of intrinsic donor defects. On the other hand, CdS nanostructures normally are single crystalline with very little defects, leading to the highly insulative feature of the unintentionally doped CdS nanostructures, which will inevitably hinder their applications in nano-optoelectronic devices. To overcome this difficulty, appropriate doping is much desired to tailor the energy band structure and tune the transport properties of the CdS nanostructures. Although efficient n-type doping on CdS thin films has been achieved by

[3] Author to whom any correspondence should be addressed.

using In and Cl as n-type dopants via various methods such as thermal evaporation [10, 11], spray pyrolysis [12], chemical bath deposition (CBD) [13, 14], post-annealing [15] and so on, controlled doping on CdS nanostructures remains a major challenge and is rarely reported [16].

Herein, we reported *in situ* Cl doping of single-crystal CdS NWs by using $CdCl_2$ as the n-type dopant via the thermal co-evaporation method. Electrical measurements conducted on single CdS:Cl NWs revealed that the conductivities of the NWs could be tuned in a wide range of five orders of magnitude by adjusting the doping concentration. Significantly, the photoconductive properties of the Cl-doped CdS NWs were significantly improved compared with the undoped ones, revealing promising applications of CdS:Cl NWs in high-performance nano-optoelectronic devices.

2. Experimental details

Cl doping of CdS NWs was carried out in a conventional tube furnace with a horizontal alumina tube, which has three independent heating zones. In a typical experiment, 0.5 g CdS powder (99.99%, Aldrich) was placed in an alumina boat and then inserted into the middle heating zone of the furnace. $CdCl_2{\cdot}2.5H_2O$ powder (AR, Shanghai Chemical Reagents Co.) was used as the Cl dopant and pre-heated at 200 °C for 2 h in nitrogen atmosphere to eliminate the crystalline water. Then the dry $CdCl_2$ powder was loaded in another alumina boat and located in the first heating zone, which is in the upstream position of the CdS source. Silicon substrates coated with 3 nm Au catalyst were placed at the downstream position ∼10 cm distance from the CdS source. The reaction chamber was then flushed and filled with a mixture gas of 50 sccm Ar and H_2 (5% in volume) after it was evacuated to a base pressure of 6×10^{-3} Pa. The pressure in the tube was adjusted to 300 Torr before heating. The $CdCl_2$ and the CdS sources were then heated up to 300–500 °C and 850 °C, respectively, and maintained at that temperature for 2 h. The Cl doping concentration was controlled by adjusting the evaporation temperature of the $CdCl_2$ source and, consequently, the vapor pressure of $CdCl_2$. After the system was cooled to room temperature, the Si substrates were taken out of the furnace and a layer of yellow wool-like product was observed on their surface. Intrinsic CdS NWs were also synthesized under the same conditions except $CdCl_2$ was not used for comparison.

Morphologies and structures of the as-synthesized CdS:Cl NWs were characterized by x-ray diffraction (XRD, Rigaku D/Max-γB, with Cu Kα radiation), field-emission scanning electron microscopy (FE-SEM, Philips XL 30 FEG) and high-resolution transmission electron microscopy (HRTEM, JEOL-2010). Compositions of the CdS:Cl NWs were detected by energy-dispersive x-ray spectroscopy (EDX, attached to the SEM) and x-ray photoelectron spectroscopy (XPS, VGESCALAB MKII). Room-temperature photoluminescence (PL) spectra were obtained by using a 325 nm He–Cd laser as the excitation source (LABRAM-HR).

To assess the electrical and photoconductive properties of the CdS:Cl NWs, nano-FETs based on individual CdS:Cl NWs were constructed. The as-synthesized CdS:Cl NWs were dispersed uniformly onto SiO_2 (300 nm)/p^+-Si substrates at a desired density. Then e-beam evaporation was employed to define the In (80 nm)/Au (20 nm) double-layer electrodes on single NWs by using a shadow mask consisting of 5 μm thick tungsten wires. Electrical measurements were performed on a semiconductor characterization system (Keithley 4200-SCS) and the white light from optical microscopy on a probe station was used as the light source to measure the photoconductive properties of the CdS:Cl NWs.

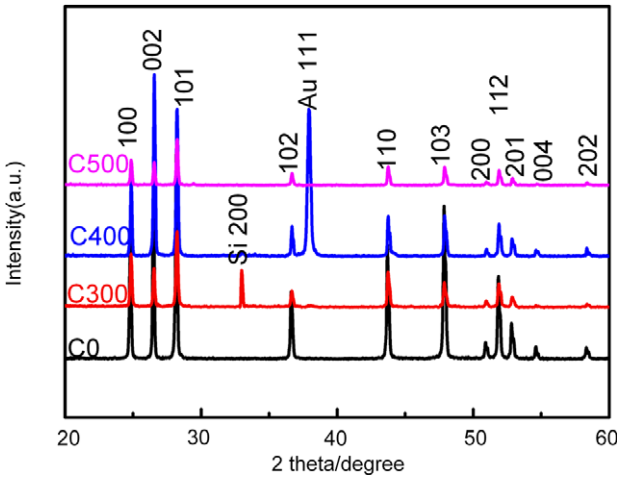

Figure 1. XRD patterns of both the intrinsic CdS NWs (C0) and the CdS:Cl NWs with increasing doping concentration from C300 and C400 to C500.

3. Results and discussions

In this work, four samples with different doping levels were synthesized, which were denoted as C0, C300, C400 and C500, corresponding to the intrinsic CdS NWs and Cl-doped CdS NWs with different $CdCl_2$ source temperatures of 300, 400 and 500 °C during NW growth, respectively. Figure 1 depicts the XRD patterns of the four samples. Except for two diffraction peaks coming from the Si substrate and the Au catalyst, all the diffraction peaks can be assigned to wurtzite CdS (JCPDS no. 41-1049), suggesting the high phase purity of the product. As compared to the undoped sample, no obvious peak broadening and peak shifts are observed for the Cl-doped CdS NWs, which can be attributed to the similar ionic radius of Cl^- (1.81 Å) to S^{2-} (1.84 Å).

Figure 2(a) shows the typical FE-SEM image of the CdS:Cl NWs. It is seen that the product is uniform and consists of a large amount of NWs with diameters in the range of 50–200 nm and lengths up to several tens of micrometers. The TEM image of a single CdS:Cl NW also reveals that the NW surface is clean and the diameter is uniform along the NW length (figure 2(b)). From the EDX spectrum (inset in figure 2(a)), the atomic ratio of Cd:S is estimated to be about 51:49, which is very close to the stoichiometric ratio of CdS. The single-crystal nature of the CdS:Cl NW is confirmed by the HRTEM image (figure 2(c)) and the corresponding selected-area electron diffraction (SAED) pattern (inset in figure 2(b)).

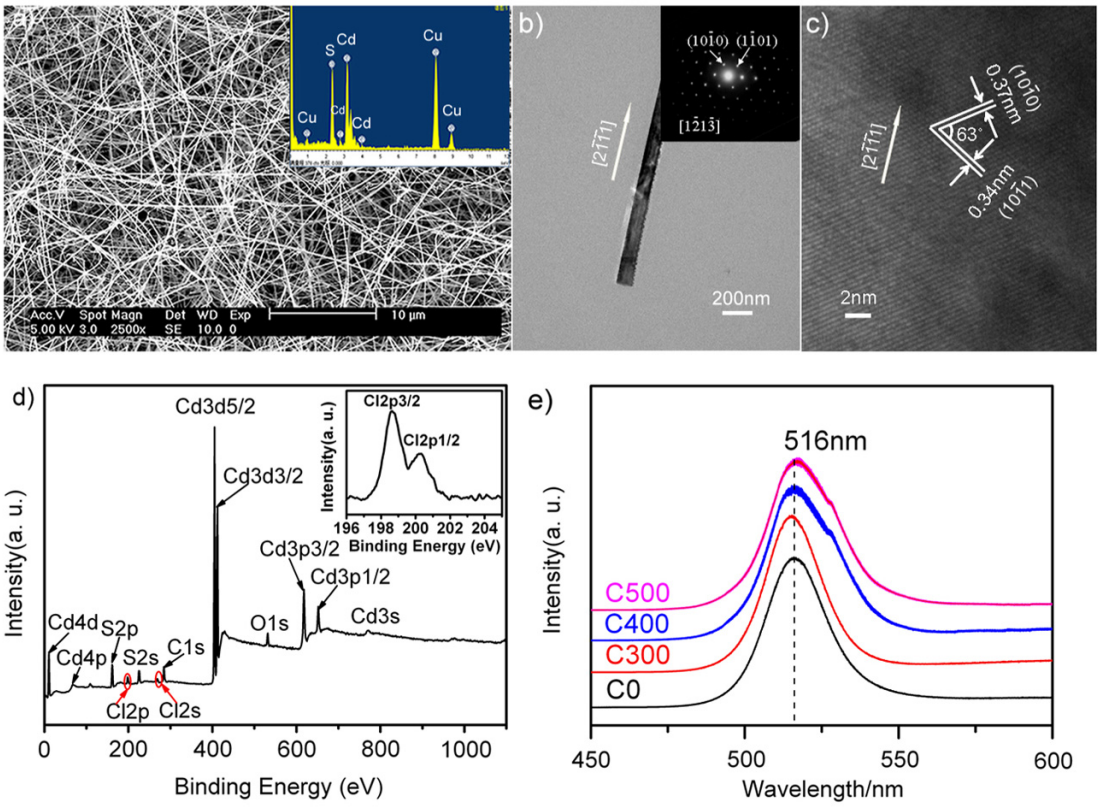

Figure 2. (a) A typical FE-SEM image of the CdS:Cl NWs. Inset shows the EDX spectrum. (b) Low-resolution TEM image of the CdS:Cl NW. Inset shows the corresponding SAED pattern. (c) HRTEM images of the CdS:Cl NW. (d) XPS spectrum of the CdS:Cl NWs. Inset shows the enlarged Cl 2p peaks. (e) Room-temperature PL spectra of both the Cl-doped and undoped CdS NWs.

Lattice spacings of 0.37 nm and 0.34 nm in the HRTEM image are consistent with the (10$\bar{1}$0) and (1$\bar{1}$01) lattice faces of wurtzite CdS, respectively. Further analysis indicates a [2$\bar{1}\bar{1}$1] growth direction for the CdS:Cl NW. It is noted that all the samples, including the doped and the undoped CdS NWs, have shown similar morphologies and crystal structures.

XPS was used to detect the compositions of the CdS:Cl NWs (from C400), as shown in figure 2(d). In addition to the peaks coming from Cd and S, two weak peaks that correspond to the Cl 2p and Cl 2s core level emission can be observed, indicating the presence of Cl element in the sample. Considering that the CdS:Cl NW product is uniform and clean with very few impurities and particles, the Cl signal is most likely coming from the Cl elements that were successfully incorporated into the CdS NWs. Figure 2(e) depicts the room-temperature PL spectra of the CdS:Cl NWs and the PL spectrum from the undoped CdS NWs is also measured for comparison. A dominant emission band corresponding to the near-band-edge (NBE) emission of CdS at 516 nm is observed for all of the samples. It is noted that the PL spectra for the CdS:Cl NWs are nearly identical to that of the undoped NWs except for the small broadening of the emission peaks, implying the crystalline quality and structural integrity of the CdS:Cl NWs are not significantly degraded by Cl incorporation.

Electrical measurements were performed to determine the doping effects of Cl on the transport properties of CdS NWs. The typical I–V curves of samples C0, C300, C400 and C500 measured in the dark are plotted in figure 3(a). We note that the intrinsic CdS NWs have the lowest conductivity of 4.3×10^{-8} S cm^{-1}, while the conductivity is remarkably enhanced for the Cl-doped CdS NWs, which increases to 4.3×10^{-6} S cm^{-1}, 4.9×10^{-5} S cm^{-1} and 3.1×10^{-4} S cm^{-1} for C300, C400 and C500, respectively. To gain statistical significance, we calculated the conductivity of 20 NWs for each sample and the corresponding histogram is depicted in figure 3(b). It is seen that the intrinsic CdS NWs have a relatively narrow conductivity distribution of $\sim 5 \times 10^{-9}$–5×10^{-8} S cm^{-1}. The conductivity distribution is slightly widened for the CdS:Cl NWs due to the uneven doping, which is $\sim 1 \times 10^{-7}$–5×10^{-6} S cm^{-1}, $\sim 1 \times 10^{-5}$–1×10^{-3} S cm^{-1} and $\sim 1 \times 10^{-4}$–5×10^{-3} S cm^{-1} for C300, C400 and C500, respectively. Notably, the conductivity of the CdS NWs can be tuned in a wide range of $\sim$5 orders of magnitude by adjusting the Cl doping concentration. The enhancement of the CdS NW conductivity can be attributed to the generation of Cl shallow donor levels below the conduction band when S atoms were substituted by the Cl dopants [17]. On the other hand, with the increasing of the evaporation temperature of the $CdCl_2$ source during NW growth, the vapor pressure of the $CdCl_2$ dopant will increase accordingly, leading to the higher Cl doping concentration and thus larger NW conductivity. However, we also note that no product could be obtained if the temperature of the $CdCl_2$ dopant is higher than its melting point (568 °C).

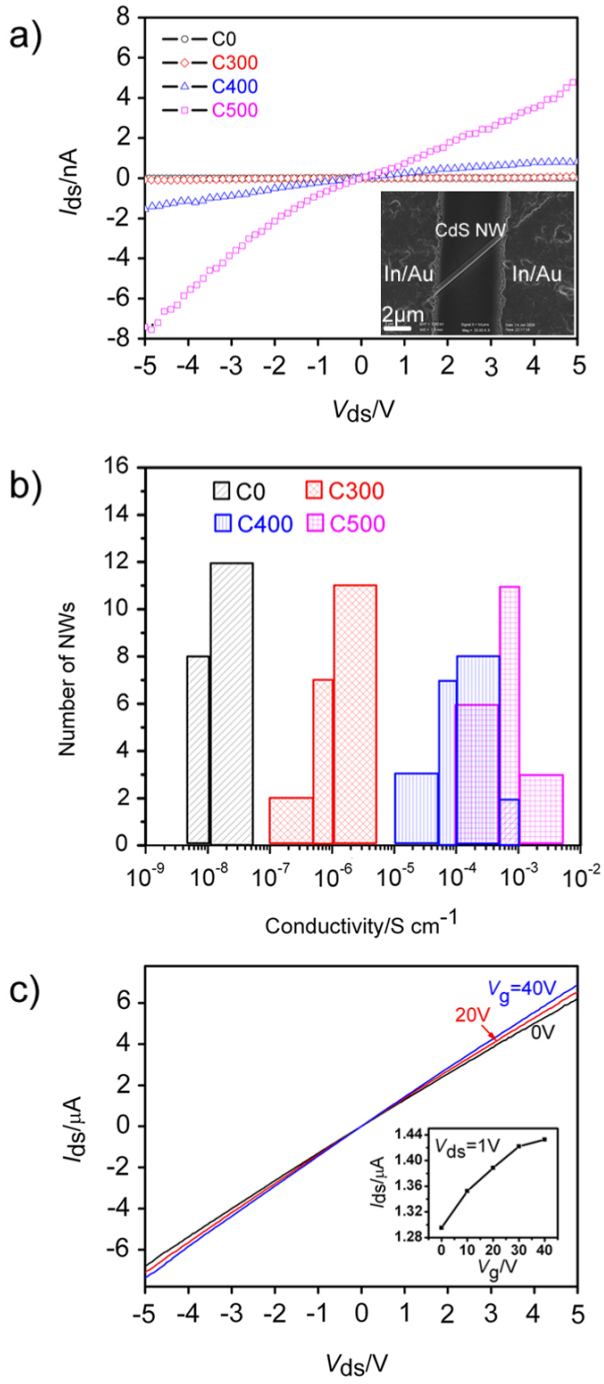

Figure 3. (a) Typical I_{ds}–V_{ds} curves of CdS NWs with varied doping concentration in dark. The inset shows the SEM image of a typical device based on a single CdS:Cl NW. (b) Distribution of conductivity values for 80 devices, 20 devices each for C0, C300, C400 and C500. (c) I_{ds}–V_{ds} curves of CdS:Cl NW (C400) measured at varied V_g. V_g increases from 0 to 40 V in steps of 20 V. Inset shows the I_{ds}–V_g curve at $V_{ds} = 1$ V.

The suppression of NW nucleation and growth at high $CdCl_2$ vapor pressure is likely responsible for this result.

The transport properties of the CdS:Cl NWs are further studied by measuring the device characteristics of the NW FET. Figure 3(c) depicts the typical gate-dependent source–drain current (I_{ds}) versus source–drain voltage (V_{ds}) curves of sample C400 measured at varied gate voltage (V_g) from 0 to 40 V. V_g was applied to the degenerate doped Si substrate, which serves as the global back-gate in the nano-FET. The measurements were conducted in light to lower the contact barrier and thus enhance the gating effect. It is found that the conductance of the CdS:Cl NW increases with increasing V_g, which is consistent with the typical behavior of an n-channel metal–oxide–semiconductor FET (MOSFET), revealing the n-type nature of the Cl-doped CdS NWs. Moreover, the field-effect mobility and electron concentration of the CdS:Cl NWs can be deduced from the electrical characteristics according to the following equations as

$$\mu_{\text{eff}} = \frac{\mathrm{d}I_{\text{ds}}}{\mathrm{d}V_{\text{g}}} \frac{\ln(4h/d)L}{2\pi\varepsilon_0\varepsilon_{\text{SiO}_2}} \tag{1}$$

$$n = \sigma/\mu_e e \tag{2}$$

where the $\mathrm{d}I_{ds}/\mathrm{d}V_g$ is extracted from the linear region of the transconductance, ε_{SiO_2} is the dielectric constant of the gate SiO_2 (3.9), L, h and d represent the NW channel length, gate oxide layer thickness and NW diameter, respectively, n is the carrier concentration and σ is the conductivity of the NW. Based on the above equations, $\mu_{\text{eff}} \approx 1.8$ cm^2 V^{-1} s^{-1} is obtained from the I_{ds}–V_g curves in figure 3(c). The carrier concentration n is calculated to be $\sim 1.1 \times 10^{18}$ cm^{-3} in light. If assuming the mobility in the dark is identical to that in light for the CdS:Cl NW, a much lower carrier concentration of $\sim 1.4 \times 10^{14}$ cm^{-3} in the dark could be obtained. We note that the CdS:Cl NW nano-FETs have exhibited relative low device performance, which can be attributed to the weak gate–channel couple caused by the back-gate device structure and the thick SiO_2 gate dielectric [7]. It is expected that the device performance could be further improved by optimizing the device architecture such as using the top-gate structure and high-k dielectric.

CdS nanostructures are promising materials for visible light detection and have important applications in nano-optoelectronics. The photoconductive properties of the Cl-doped CdS NWs are investigated in this study to further evaluate the impact of doping. Figure 4(a) shows the typical I–V curves of the four samples measured under light illumination (white light from optical microscopy, 0.35 mW cm^{-2}). Significantly, the conductivity of the NWs shows a pronounced increase up to 3–4 orders of magnitude upon light illumination, which increases to $\sim 3.7 \times 10^{-5}$ S cm^{-1} for sample C0, ~ 0.01 S cm^{-1} for sample C300, ~ 0.38 S cm^{-1} for sample C400 and ~ 0.60 S cm^{-1} for sample C500. The statistical histogram of the photoconductivity for sample C400 is shown in figure 4(b). All the CdS:Cl NWs counted exhibit an obvious increase in the photoconductivity, revealing the high uniformity of the samples. Figures 4(c) and (d) depict the time response spectra of the CdS:Cl NW (C400) and the intrinsic CdS NW (C0), respectively. Both the doped and undoped CdS NWs show excellent stability and reproducibility with a fast response time less than 1 s (limited by the speed of manually turning on and off the light). It has been suggested that the trapping centers, such as the defects introduced by the doping process, will result in the decrease of the photo-response speed [18]. Our result implies that the CdS:Cl NWs

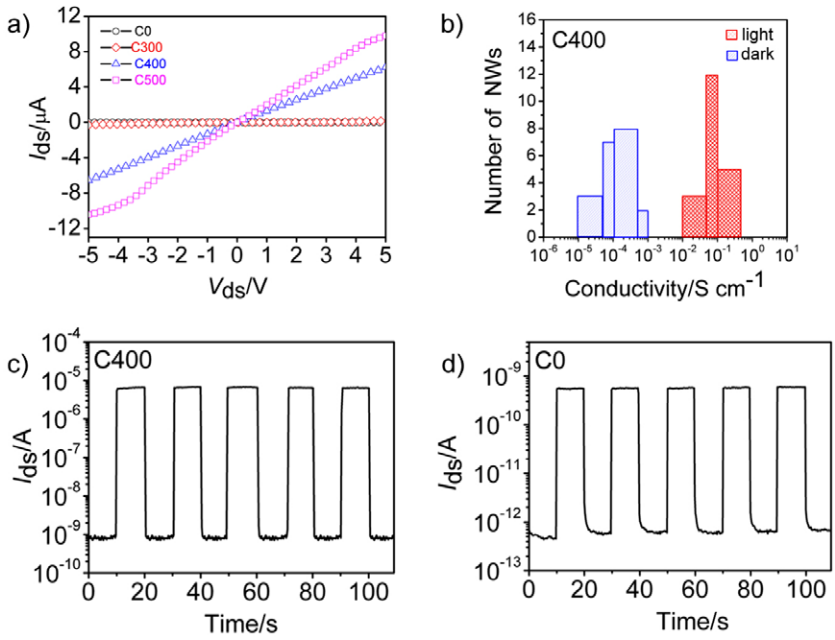

e)

	R(AW^{-1})	G	I_{light} / I_{dark}
C0	0.18	0.48	~10^3
C300	54.6	144	~2×10^3
C400	1.9×10^3	5×10^3	~7×10^3
C500	3×10^3	7.8×10^3	~2×10^3

Figure 4. (a) Typical I_{ds}–V_{ds} curves of single CdS NWs with varied doping concentrations measured under white light illumination (0.35 mW cm^{-2}). (b) Conductivity distribution of 20 CdS:Cl NWs (C400) in dark and in light. Time response of (c) sample C400 and (d) sample C0. The LED white light from the microscope was turned on/off manually. V_{ds} was fixed at 5 V. (e) The table summarizes the key parameters include R, G and I_{light}/I_{dark} ratio for both the doped and undoped CdS NWs. G is calculated by assuming $\eta = 1$ for simplification and the central wavelength of the LED light of 470 nm is used.

have high crystal quality and therefore their response speed can as fast as the undoped ones. From the response spectra, the I_{light}/I_{dark} ratio for C400 is estimated to be $\sim 7 \times 10^3$, in contrast to the lower value of $\sim 10^3$ for C0. It is noted that the I_{light}/I_{dark} ratio first increases from C0 to C400 and then decreases for C500. The increase in the I_{light}/I_{dark} ratio can be attributed to the enhancement of photocurrent, while the decrease of it for C500 is likely due to the large dark current at high doping concentration. Based on our results, a balance between the doping level and the device performances should be taken. On the other hand, we note that the most significant difference between the doped samples and C0 is the photocurrent, which is 6.23 μA for C400 but only 6 nA for C0 under the same light illumination at $V_{ds} = 5$ V. This difference can be quantitatively described by responsivity (R), which is a key parameter for a photodetector and reflects the sensitivity of the photodetector to the incident light. R is defined as [19]

$$R(A/W) = \frac{I_p}{P_{opt}} = \eta\left(\frac{q\lambda}{hc}\right)G \tag{3}$$

$$G = \frac{N_{el}}{N_{ph}} = \frac{\tau}{\tau_{tr}} \tag{4}$$

where I_p is the photocurrent, P_{opt} the incident light power, η the quantum efficiency, h Planck's constant, c the speed of light, λ the incident light wavelength and G the photoconductive gain, which is defined as the ratio between the number of electrons collected per unit time (N_{el}) and the number of absorbed photons per unit time (N_{ph}) or the ratio of carrier lifetime (τ) to carrier transit time (τ_{tr}). Based on the above equations, R is estimated to be 0.18 A W^{-1} for sample C0, 54.6 A W^{-1} for sample C300, 1.9 × 10^3 A W^{-1} for sample C400 and 3 × 10^3 A W^{-1} for sample C500. Accordingly, the photoconductive gain has significantly increased from ~0.48 for sample C0 to $\sim 7.8 \times 10^3$ for sample C500 (figure 4(e)). The substantial improvement of R and G for the CdS:Cl NWs could be ascribed to the presence of deep level trap states in NWs that greatly prolong the lifetime of photocarriers by preventing the electron–hole recombination [20]. Our results undoubtedly demonstrate that the photoconductive properties of the CdS

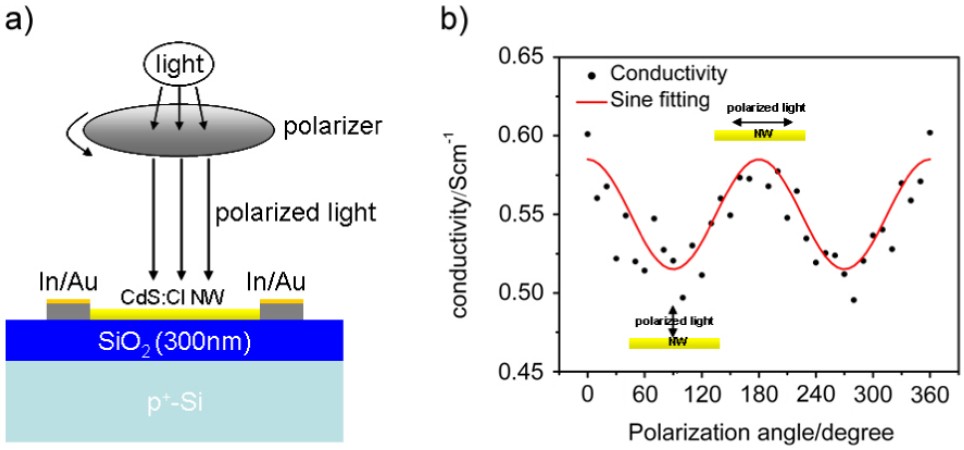

Figure 5. (a) Schematic diagram shows the measurement configuration for polarization-sensitive measurements. (b) Polarization sensitivity of CdS:Cl NW to the incident light with varied polarized angle.

NWs can be dramatically enhanced and rationally controlled by Cl doping.

The one-dimensional geometry of the NW may lead to the polarization-sensitive absorption of the incident light. In this work, we further study the effect of polarization sensitivity on the photoconductive properties of the CdS:Cl NWs, as shown in figure 5. The polarized light is generated by using a polarizer, which can be rotated to continually change the polarization angle with respect to the longitudinal orientation of the NW. Significantly, the photoconductivity of the CdS:Cl NW exhibits strong dependence on the polarization angle and a relationship like a sine wave could be deduced by fitting the data. When the light is longitudinally polarized with respect to the NW, the photoconductivity of the NW reaches a maximum, in contrast to the smaller photoconductivity with transversely polarized light and a conductivity difference up to 12% is revealed. According to the previous investigation by Mencarelli *et al* on carbon nanotubes [21], the polarization-sensitive absorption can be responsible for this phenomenon. The polarization-dependent photocurrent of the CdS:Cl NWs may have potential applications in optoelectronic devices and optical sensors.

4. Conclusions

In summary, Cl-doped n-type CdS NWs were successfully synthesized by using $CdCl_2$ as the dopant via a thermal co-evaporation method. The CdS:Cl NWs have wurtzite single-crystal structure with a growth direction of $[2\bar{1}\bar{1}1]$. It is found that the conductivity of the CdS:Cl NWs can be tuned in a wide range of five orders of magnitude by adjusting the Cl doping concentration. Moreover, nano-photodetectors fabricated from the CdS:Cl NWs exhibit excellent stability and reproducibility and have a response speed as fast as the undoped ones. Significantly, the photoconductivity of the CdS NWs is greatly enhanced by Cl doping. The responsivity and photoconductive gain of the CdS:Cl NWs have increased by four orders of magnitude as compared with the undoped ones. On the other hand, the CdS:Cl NWs also show strong polarization-dependent photoconductivity. The ability to tune the electronic and optoelectronic properties of CdS NWs by Cl doping opens the opportunities for high-performance nano-optoelectronic devices based on CdS nanostructures.

Acknowledgments

This work was supported by the National High Technology R&D Program of China (863 Program) (no. 2007AA03Z301), the National Natural Science Foundation of China (NSFC, nos. 60806028 and 2090102), the Program for New Century Excellent Talents in Universities of the Chinese Ministry of Education (no. NCET-08-0764) and the Special Foundation for Doctors of Hefei University of Technology (no. 2007GDBJ028).

References

[1] Liu Y K, Zapien J A, Geng C Y, Shan Y Y, Lee C S, Lifshitz Y and Lee S T 2004 *Appl. Phys. Lett.* **85** 3241
[2] Jie J S, Zhang W J, Jiang Y, Meng X M, Li Y Q and Lee S T 2006 *Nano Lett.* **6** 1887
[3] Liu Y K, Zapien J A, Shan Y Y, Geng C Y, Lee C S and Lee S T 2005 *Adv. Mater.* **17** 1372
[4] Duan X F, Huang Y, Agarwal R and Lieber C M 2003 *Nature* **421** 241
[5] Ye Y, Dai L, Wu P C, Liu C, Sun T, Ma R M and Qin G G 2009 *Nanotechnology* **20** 375202
[6] Nagasaki Y, Ishii T, Sunaga Y, Watanabe Y, Otsuka H and Kataoka K 2004 *Langmuir* **20** 6396
[7] Jie J S, Zhang W J, Bello I, Lee C S and Lee S T 2010 *Nano Today* **5** 313
[8] Jie J S, Zhang W J, Jiang Y and Lee S T 2006 *Appl. Phys. Lett.* **89** 223117
[9] Wu D, Jiang Y, Wang L, Li S Y, Wu B, Yu Y Q, Wu C Y, Wang Z B and Jie J S 2010 *Appl. Phys. Lett.* **96** 123118
[10] George P J, Sanchez A, Nair P K and Nair M T S 1995 *Appl. Phys. Lett.* **66** 3624
[11] Abu-Safe H H, Hossain M, Naseem H, Brown W and Al-Dhafiri A 2004 *J. Electron. Mater.* **33** 128

[12] Valdna V 1999 *Solid State Phenom.* **309** 67
[13] Hiie J, Dedova T, Valdna V and Muska K 2006 *Thin Solid Films* **511** 443
[14] Osipyonok N M, Singaevsky A F, Noskov Y V, Piryatinski Y P, Smertenko P S, Dimitriev O P and Pudb A A 2008 *Mater. Sci. Eng.* B **147** 254
[15] Kokaj J and Rakhshani A E 2004 *J. Phys. D: Appl. Phys.* **37** 1970
[16] Ma R M, Dai L, Huo H B, Yang W Q, Qin G G, Tan P H, Huang C H and Zheng J 2006 *Appl. Phys. Lett.* **89** 203120
[17] Gao T, Li Q H and Wang T H 2005 *Appl. Phys. Lett.* **86** 173105
[18] He Z B, Jie J S, Zhang W J, Zhang W F, Luo L B, Fan X, Yuan G D, Bello I and Lee S T 2009 *Small* **5** 345
[19] Liu K W, Ma J G, Zhang J Y, Lu Y M, Jiang D Y, Li B H, Zhao D X, Zhang Z Z, Yao B and Shen D Z 2007 *Solid-State Electron.* **51** 757
[20] Soci C, Zhang A, Xiang B, Dayeh S A, Aplin D P R, Park J, Bao X Y, Lo Y H and Wang D 2007 *Nano Lett.* **7** 1003
[21] Mencarelli D, Pierantoni L and Rozzi T 2008 *J. Appl. Phys.* **103** 063013